J Low Temp Phys (2012) 169:208–217
DOI 10.1007/s10909-012-0641-4

NMR Study of Disordered Inclusions in the Quenched Solid Helium

A.P. Birchenko · N.P. Mikhin · E.Y. Rudavskii · Y.O. Vekhov

Received: 9 March 2012 / Accepted: 28 May 2012 / Published online: 7 June 2012

Abstract Phase structure of rapidly quenched solid helium samples is studied by the NMR technique on dilute ^{3}He–^{4}He mixtures. The pulse NMR method is used for measurements of spin–spin T_2 relaxation time and spin diffusion coefficient D for all coexisting phases. It was found that quenched samples are two-phase systems consisting of the hcp matrix and some inclusions which are characterized by D and T_2 values close to those in liquid phase. Such liquid-like inclusions undergo a spontaneous transition to a new state with anomalously short T_2 times. It is found that inclusions observed in both the states disappear on careful annealing near the melting curve. It is assumed that the liquid-like inclusions transform into a new state—a glass or a crystal with a large number of dislocations. These disordered inclusions may be responsible for the anomalous phenomena observed in supersolid region.

Keywords Solid helium · NMR · Metastable inclusions · Supersolid

1 Introduction

The search for the supersolid state in solid helium has recently led to the detection of anomalous behavior first in torsional experiments [1] and then in investigations of elastic properties [2], specific heat [3], and mass transfer [4]. Although the effects observed are still waiting for a consistent explanation, the anomalies are most often credited to some type of disorder that can develop in a solid. For example,

A.P. Birchenko · N.P. Mikhin · E.Y. Rudavskii · Y.O. Vekhov (✉)
Department of Quantum Fluids and Solids, B. Verkin Institute for Low Temperature Physics and Engineering of the National Academy of Sciences of Ukraine, 47 Lenin Ave., Kharkov 61103, Ukraine
e-mail: yegor_v@ukr.net

these may be a system of dislocations, grain boundaries, liquid inclusions or a disordered (glassy) phase. To understand the phenomenon of supersolid, it is fundamentally important to identify the conditions creating disorder in solid helium and the properties of the appearing disordered phase.

Much research has been carried out along this line employing various theoretical and experimental methods. The Monte-Carlo simulations [5, 6] support the view that the supersolid state is impossible in a perfect hcp crystal of ^{4}He. However, the signs of a disordered glassy phase were detected in torsion experiments investigating relaxation dynamics [7, 8]. A large contribution from a disordered (glassy) phase to the pressure of ^{4}He crystals grown by fast cooling [9] and samples deformed *in situ* [10] was registered by precise barometry. The contribution of a glassy phase to the properties of solid helium was calculated in Refs. [11, 12]. Interesting information was derived from visual observation of the disorder in solid ^{4}He [13]: the samples grown by the blocking capillary method were polycrystals with micrometer size grains, and the liquid phase may well exist at the grain boundaries.

Information about the phase composition of a sample can be obtained by the method of nuclear magnetic resonance (NMR) on ^{3}He impurities. For example, the investigations of spin diffusion in a region of a bcc-hcp transition [14] revealed an additional diffusive process in a sample in which both crystallographic phases coexisted. The process is characterized by high diffusion coefficients and indicated that liquid-like inclusions can form in the sample in the course of the bcc-hcp transition. Later the presence of such inclusions in pure ^{4}He and dilute ^{3}He–^{4}He solid mixtures was confirmed by precise pressure measurements [14, 15]. The subsequent NMR investigations of the hcp phase [16] showed that regions with high diffusion coefficients appeared readily in fast-grown single-phase samples. It was found that in addition to the high diffusion coefficient, the inclusion had spin–spin relaxation times which are inherent in the liquid phase [17]. The detected liquid-like inclusions disappeared after thorough annealing.

This study, which is a continuation of the previous NMR experiments [16, 17], is concentrated on a detailed investigation of the revealed non-equilibrium phase. It is focused on identification of coexisting phases rather than the study of kinetics of the occurring processes.

Since NMR measurements in helium are usually made on ^{3}He nuclei with a nonzero magnetic moment, a ^{4}He crystal for this investigation must contain a certain amount of the ^{3}He impurity. It is especially important for measurements in the region of supersolid effects (below $\sim$300 mK) because the anomalies in question are sensitive even to low concentrations of the ^{3}He impurity. That is why the NMR experiments performed at very low temperatures [18–21] could furnish important information about the state of ^{3}He in the supersolid region.

Our NMR measurements were made at high temperatures (above $\sim$1.3 K) to pursue another objective: to use ^{3}He atoms as probes for identifying and investigating the metastable (disordered) phase in solid helium, keeping in the mind that any thermodynamical phase of ^{3}He–^{4}He mixture is characterized by specific values of diffusion coefficient and NMR relaxation times T_1 and T_2 (see Ref. [17]).

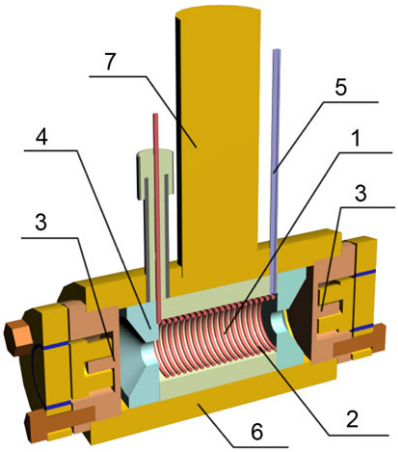

Fig. 1 Schematic view of a NMR cell: *1*—cell cavity; *2*—NMR coil; *3*—pressure gauges (BeCu); *4*—fluoroplastic displacers; *5*—cell filling capillary; *6*—cell body (Cu); *7*—cooling finger (Color figure online)

2 Experimental Technique

The experimental cell used for NMR measurements in solid helium is shown schematically in Fig. 1. The cell cavity (1) in the form of a cylinder 16 mm long and 8 mm in diameter was filled with helium. NMR coil (2) was wound in the inner surface of the cavity (sample). Straty-Adams pressure gauges (3) of ±5–10 mbar resolution were fixed at the cylinder ends. They were separated from the cylinder cavity with specially designed fluoroplastic displacers (4) to reduce edge effects on the NMR signal. The filling capillary (5) of the cell was made of stainless steel of 0.1 mm inner diameter. It was thermally connected to a 1K-pot to apply the blocking capillary method of growing solid helium samples. A resistance thermometer was mounted on the copper body (6) of the cell to measure the sample temperature (it had an accuracy of ±5 mK and a sensitivity of ±1 mK). The thermostabilizing system (heater and thermometer) attached in the upper part of a copper cooling finger (7) ensured temperature stabilization within ±1 mK. The systems of thermometry, thermostabilization, barometry, and NMR measurements were completely automated.

The measurements were made in the temperature range $1.3 - 1.8$ K.[1] The hcp crystals under investigation corresponded to the pressures 34–40 bar ($V_m = 20.3 - 20.0$ cm^3/mol), i.e. were grown from the normal liquid above the upper triple point (bcc-hcp-He I). The crystals were obtained by fast cooling along the melting curve at a rate of ∼2–6 mK/s, which produced a large number of defects in the sample. Under such conditions the sample of solid helium also contains a large number of liquid-like inclusions that might be captured under crystallization (see Ref. [17]).

The experiments were performed with a solid ^{3}He–^{4}He mixture with a concentration of 1.0 ± 0.05 % ^{3}He. In our previous experiments [17, 22] we studied in detail both the phase diagram and kinetic characteristics (diffusion coefficient, spin–lattice and spin–spin relaxation times) in equilibrium phases of this concentration. In

[1] This temperature range is enough high to avoid as phase separation of solid mixture as ^{3}He pinning on edge dislocation cores which are usually observed at much lower temperatures. Spin-lattice relaxation time T_1 here is also still enough short for reasonable promptly NMR measurements.

addition, the phase diagram of the mixture with such concentration does not differ essentially from the diagram of pure ^{4}He.

The initial concentration has been prepared by mixing the helium isotopes in gaseous phase, and the concentration in the crystal under investigation is checked using comparison of the NMR amplitudes in the mixture and in pure ^{3}He. The difference in the ^{3}He concentration between crystalline and liquid phases [23] is essential at temperatures below those used in this study.

The nuclear magnetic relaxation times and the spin diffusion coefficients were measured in the NMR experiments. The measurements were made at the frequency $f_0 = 9.15$ MHz using sequences of probe pulses (the Carr-Purcell (*PC*) method) $90° - \tau - 180°$ [24], where τ is the time interval between the pulses.

The time of spin–spin relaxation T_2 and the spin diffusion coefficient D were estimated by measuring the dependence of the relative echo-signal amplitude h/h_0 on the time interval τ between the probe pulses. In the *CP* method, this dependence is [24]:

$$\frac{h}{h_0} = \sum_i \alpha_i \left[1 - \exp\left(\frac{\Delta t}{(T_1)_i}\right)\right] \exp\left[-\frac{2\tau}{(T_2)_i} - \frac{2}{3}\gamma^2\tau^3 G^2 D_i\right], \tag{1}$$

where Δt is the time interval between the pulse sequences, G is the magnetic field gradient, $(T_1)_i$ is the time of spin–lattice relaxation in the i-th phase, $(T_2)_i$ is the time of spin–spin relaxation in the i-th phase, D_i and α_i are the diffusion coefficient and the relative volume content of the i-th phase, respectively; γ is the gyromagnetic ratio. T_1, T_2, and D can be found by varying the corresponding parameters in (1). The time of spin–lattice relaxation, T_1, can be obtained from the dependence $h/h_0(\Delta t)$ on varying Δt, the other parameters being constant. The spin–spin relaxation time, T_2, can be obtained from the dependence $h/h_0(\tau)$ which is measured under the lowest magnetic field gradient (G is close to zero) on varying τ and holding Δt constant. Finally, the diffusion coefficient, D, is derived from the dependence $h/h_0(\tau)$ under a non-zero magnetic field gradient with constant Δt.

If the system contains several subsystems (coexisting phases), (1) gives a sum of the corresponding exponents, and sought-for kinetic coefficients are obtainable from the analysis which was proved to be reliable from NMR experiments in the single-phase regions of the mixture. They agree with available data for mixtures of 1.94 % ^{3}He for relaxation times [25, 26], 0.75 % and 2.17 % ^{3}He for diffusion coefficients [27, 28] taking into account the difference in the ^{3}He concentrations. Thus, we used results of NMR measurements for authentication of coexisting thermodynamics phases. The phase transition kinetics between the coexisting phases is not a subject of this work.

3 Anomalous Behavior of Spin–Spin Relaxation Time

The analysis of T_1-, T_2-, and D-values shows that the parameter T_2 (spin–spin relaxation time) and D (diffusion coefficient) [16, 17] can provide an information necessary for identifying the phase structure of the sample. T_2 can tell about the changes of

the intensity of the spin motion. Such information was used to investigate the properties of solid helium in [29, 30]. According to the Bloembergen-Purcell-Pound (BPP) model [31], the rate of spin–spin relaxation decreases as the intensity of the relative motion of nuclei with a non-zero magnetic moment (^{3}He nuclei) increases. This correlation between T_2 and D was quite fully considered in [32]. On the other hand, when there are no additional strong magnetic effects (e.g. ferro- and diamagnetic impurities [33]) T_2, unlike D, is independent of the shape and the size of fine-grained objects. It is therefore appropriate to discuss the results obtained beginning with the time T_2.

The starting experimental dependences $h/h_0(\tau)$ taken on the same crystal in several states are illustrated in Fig. 2. The as-grown hcp crystal obtained on cooling along the melting curve at the rate of ∼5 mK/s is shown in Fig. 2a. The dependence $h(\tau)$ has two slopes corresponding to two processes—fast relaxation with the time $T_2 = 36 \pm 21$ ms and slow relaxation with the time $T_2 = 362 \pm 62$ ms. T_2 for the fast process measured at $T = 1.7$ K is consistent with the spin–spin relaxation time for a bulk liquid at $P \sim 25$ bar; in the case of the slow process this time corresponds to the hcp phase. These data for the single-phase states of the investigated system were obtained in special calibration experiments [17]. They support our previous conclusion [16, 17] that metastable liquid-like inclusions are formed readily in fast grown crystals of solid helium.

An unexpected effect was observed in the course of NMR measurements when a fast grown sample with metastable liquid-like inclusions was investigated for about three hours at $T = 1.7$ K. In this case the obtained dependence $h/h_0(\tau)$ is also a superposition of two exponents (Fig. 2b), where the time T_2 for the hcp phase is now 443 ± 51 ms (within the total experimental error it can be taken as practically unchanged). The time T_2 for the fast process connected with the formation of liquid-like inclusions decreased by an order of magnitude and was 3.2 ± 3.0 ms. In all the cases this change in T_2 was rather fast: it occurred within one measurement run, i.e. no longer than $\Delta t \sim 100$–300 s. It is natural to assume that the liquid-like inclusions in the hcp matrix undergo some evolution or a phase transition.

The dependences calculated with (1) (Figs. 2a and 2b) show that the weighting factor α_i for non-equilibrium inclusions (see Fig. 2b) is about three times higher than in the case of Fig. 2a (estimation of α_i is detailed in Sect. 4).

Note that the dependence $h(\tau)$ taken after thorough (∼ 2 hours) annealing of the sample near the melting curve ($T = 1.95$ K) and subsequent cooling down to $T = 1.7$ K can be described by one exponent with $T_2 = 350 \pm 19$ ms, which is characteristic of the hcp phase at this temperature (see Fig. 2c). This means that after annealing the non-equilibrium inclusions disappeared almost completely and the sample became a single-phase hcp crystal.

The similar dependences h/h_0 *vs* τ have been obtained for various temperatures in the region 1.3–1.8 K. In Fig. 2 we presented only the data at 1.7 K because it is typical behavior observed during this transition from the liquid droplets to a new state. Figure 3 presents the data for the inclusions in a new state for whole temperature region. Figure 3 shows also the experimental data for the single-phase states of the system—the liquid and the hcp phases (see Ref. [17]). In the liquid state T_2 is practically temperature-independent (within the scatter of experimental data) in

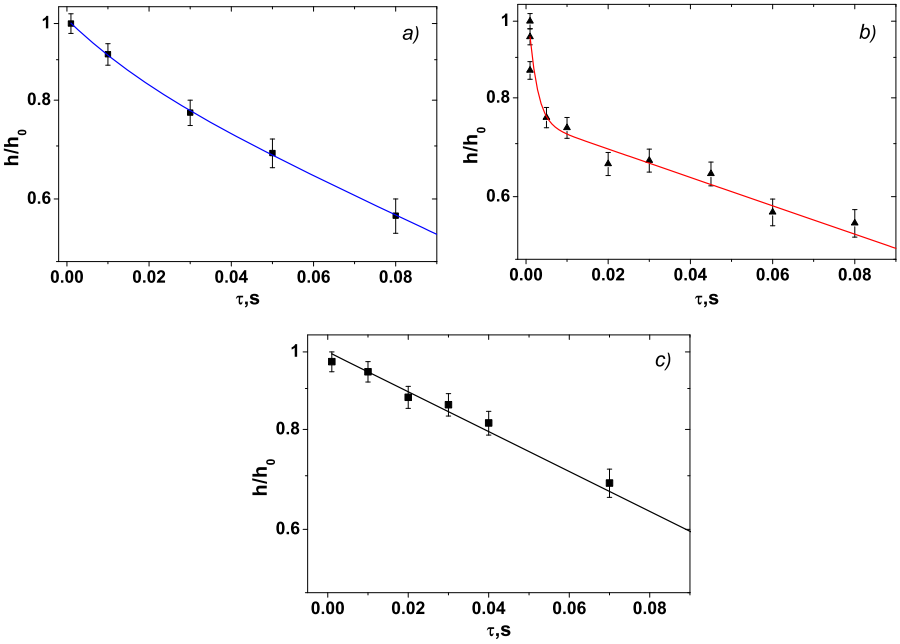

Fig. 2 The dependence of the spin–echo amplitude (in semi-log scale) on the time interval between probe pulses ($G = 0$) for different states of sample: (**a**) as-grown fast-cooled sample, $T = 1.7$ K, $P = 35$ bar ($\Delta t = 150$ s); (**b**) the same sample after isothermal 3 hour exposure ($\Delta t = 100$ s); (**c**) the same sample after annealing near the melting curve and subsequent cooling down to $T = 1.7$ K ($\Delta t = 100$ s). *Solid lines* correspond to the least square method (LSM) fitting the experimental data according to (1) (Color figure online)

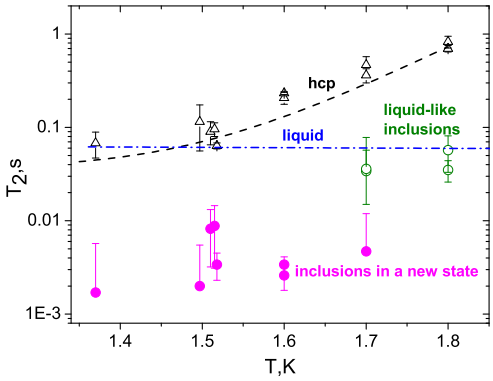

Fig. 3 The temperature dependence of the spin–spin relaxation time T_2 for: (*green* ○)—metastable liquid-like inclusions [17], (*red* ●)—metastable inclusions after their transition to a new state, (△)—time T_2 for the hcp phase in the presence of metastable inclusions. *Dashed line*—data for a single-phase hcp sample at $P \sim 35$ bar [17], *dash-dot line*—data for a bulk liquid at $P \sim 25$ bar [17] (Color figure online)

the region far from the degeneracy Fermi temperature. In the hcp phase T_2 decreases with lowering temperature and at $T \sim 1.5$ K the T_2-values of the crystal and the liquid almost coincide. The reason for this accidental coincidence is as follows: in the investigated temperature region the rate of spin–spin relaxation in the crystal is mainly determined by the concentration and the mobility of vacancies which intensify the motion of ^{3}He impurity atoms. According to the BPP theory [31], the influence of

the magnetic fields of the neighboring nuclear spins is averaged more efficiently and the spin–spin relaxation slows down. The Arrhenius equation suggests that T_2 decreases as the temperature of the crystal lowers. As a result, the contribution of the liquid-like inclusions is practically inseparable at $T < 1.7$ K.

The T_2-values measured after the transition of the liquid-like inclusions to a new state are shown in Fig. 3. They are over an order of magnitude lower than T_2 of liquid-like inclusions. Note that the transition of liquid-like inclusions to a new state was observed in most of the investigated crystals with the delay time after stabilization of the temperature varying from half an hour to several hours. The process was spontaneous and lasted during not more than 100–300 s with no distinct correlation with temperature.

4 Discussion

The spin–spin relaxation time, T_1, was measured correctly in this experiment only in the hcp phase with liquid inclusions. In this case the value of T_1 in liquid droplets is much more than that in the hcp phase $T_{1L} > T_{1HCP}$. It is very difficult to distinguish inclusions and the hcp matrix after transition of the liquid-like inclusions to the new state because $T_{1incl} \sim T_{1HCP}$.

The behavior of the diffusion coefficient D in samples grown on fast cooling is analyzed using the τ-dependences of the spin echo-signal amplitude. These dependences are a superposition of two exponents [16, 17]—a slowly attenuating exponent and a fast attenuating one which correspond to the hcp phase and the liquid-like inclusions, respectively. In this way the diffusion coefficient was found reliable only on the stage of existence of the liquid inclusions.

Note that the D-values measured for liquid-like inclusions are at least as slow as the rate of crystal growth [17]. Under the steepest rate in Ref. [16] the D-value coincided with the same rate for bulk liquid. This suggests that the size of the metastable liquid drops captured in the process of crystallization is smaller for a slower crystallization rate. This may be due to a limited diffusion, like that usually observed when the size of liquid-like inclusions is comparable to the diffusion length $\sqrt{D\tau}$ (e.g., see Ref. [34]). The value of the diffusion length according to our estimations is $\sim 10^{-3}$–10^{-2} cm. In this case the measured coefficient D is dependent on the size of the inclusions.

The situation changed as the liquid-like inclusions transformed into a new state, with anomalously short times T_2. Because of the short $T_2 \approx 7$ ms for the inclusions in the new state, the appropriate contribution to echo-signal amplitudes decays in the short run. So we could not measure the diffusion coefficient accurately even using the Hahn stimulated echo method [35], which provides measurements of the small values of D under short time of T_2. Estimates showed that the D-value for the new state is not larger than that in the hcp phase.

According to (1), correct estimation of the relative contribution of α_i to the amplitudes of the echo-signal of the coexisting phases is possible if the time intervals Δt between the sequences of probe pulses in NMR measurement are several times longer than the maximum time of spin–lattice relaxation in all phases, i.e. when magnetization is recovered completely. Only under this condition the echo signal does reach

its maximum value. This requirement is not always satisfied in real experiments because metastable inclusions evolve even during one run of D or T_2 measurement. So, magnetization of some phases are recovered incompletely during NMR measurement because of the difference in the rates of spin–lattice relaxation in the phases, and this leads to a distortion of α_i-values. The obtained α_i-values are therefore rather approximate. The estimation performed for annealed hcp samples using Δt and T_1 shows that α_i of metastable inclusions can be as high as ∼20–30 %.

The detected new phase is a long-living metastable state (see above) which disappears only after thorough annealing of the sample. Its properties differ from those of the hcp phase and liquid. We believe that the most probable reason for the decrease in T_2 of these inclusions is a transition of the liquid-like inclusions having higher diffusion coefficients to a new state with low D. The decrease in D of the liquid entails a reduction of the relaxation time T_2 (see Sect. 3). This situation is similar to solidification of a liquid without crystal order, i.e. the transition to an amorphous or glass-like state. Previously [36] the feasibility of formation of the amorphous phase in solid rare gases was found from heat capacity measurements on samples grown by condensation on a cold substrate. Unfortunately we are unaware of data on the relaxation time T_2 and the diffusion coefficient D in amorphous helium, which makes the identification of the structure of the obtained phase somewhat uncertain. This assumption was however supported by precise measurements of pressure in solid ^{4}He samples grown by fast cooling [9]. Apart from the phonon influence, an additional contribution to the pressure P_g proportional to T^2 was observed, which occurs typically in a disordered (glassy) phase. Recently, an amorphous helium phase has also been registered in neutron diffraction experiments [37]. As follows from the structural factor analysis, liquid helium confined in a porous medium holds its liquid state to the pressure $P \sim 38$ bar at $T \sim 0.4$ K and then an amorphous phase forms when liquid helium solidifies.

Crystallization of liquid-like inclusions generating a large number of dislocations can be another factor responsible for the lower T_2-values. It is known that dislocations in crystals act as centers attracting impurities. In our case this attraction enriches the regions around dislocations in ^{3}He atoms. The increasing local ^{3}He concentration reduces the time of spin–spin relaxation in this region as $T_2 = 7.5 \cdot 10^{-5}/x$ (s), where x is the relative ^{3}He concentration [30]. This dependence satisfactorily describes other authors results [25, 30, 38] and closely agrees with the calculation according to the Torrey theory [39].

There is one more scenario of a significant decrease in the time of nuclear magnetic relaxation [33]. Within a limited geometry the relaxation processes accelerate significantly in the presence of magnetic impurities on the walls. In this experiment a limited geometry could be created by crystalline dendrites growing into the volume of the liquid-like inclusions [40], and the ^{3}He atoms possessing nuclear paramagnetism could act as magnetic impurities. However, according to the Curie Law, the influence of such impurities is essential at rather low temperatures [41, 42]. It was therefore hardly probable in this experiment.[2]

[2]Prof. D.A. Tayurskii kindly indicates us that according to Ref. [43] paramagnetic ^{3}He atoms situated in microcracks at the crystal surface may play the role of effective accelerators of both spin–spin and spin–lattice relaxations.

We also considered the possibility of the formation of bcc inclusions (in the P–T phase diagram the bcc phase is quite close to the solid helium region under investigation). However, T_2 in the bcc phase is about ~ 0.1–1 s [44], which is one or two orders of magnitude higher than the times of the new state.

Note that in the course of the investigation on as-grown rapidly quenched samples both the pressure gauges in the cell exhibited a long-duration (up to 20 h) monotonic growth of pressure at a constant temperature. The rate of the pressure growth increased with the temperature, which suggests the thermally activated origin of the effect. The effect is attributed to the pressure gradient in the rapidly quenched samples. The pressure did not increase in samples grown carefully and slowly during ~ 0.5–1 h as well as after annealing.

5 Conclusion

The series of experiments in this study and Ref. [17] have shown that a disordered metastable long living phase is readily formed in fast-grown helium crystals. The new phase coexists with the equilibrium crystalline phase. The measured diffusion coefficient and the spin–spin relaxation time of this phase correspond at first to the values typical for the liquid phase. The size of the liquid-like inclusions is larger if the growth rate of the crystal is higher. The liquid-like inclusions do not form in crystals grown on cooling along the melting curve at comparatively low rates. The liquid-like inclusion disappear after thorough annealing near the melting temperature. They form at the stage of the crystal growth, and their size and quantity can be controlled by varying the growth rate of the crystal.

A new effect—a spontaneous transition of liquid-like inclusions to another state has been detected. The state has an anomalously short time of spin–spin relaxation, unusual for both a crystal and a liquid phase. It is assumed that the new state is either an amorphous (glassy) phase or a crystal with a large number of dislocations. To identify the disordered phase definitely, further experimental investigations are necessary, in particular by structural methods.

In the context of the supersolid problem it is important to allow for the influence of the disordered phase on the properties of helium crystals. It is likely that the metastable disordered inclusions with very short times of spin–spin relaxation may be responsible for the anomalous phenomena in the region of supersolid.

Acknowledgements The authors are indebted to V.A. Maidanov, V.D. Natsik, A.I. Prokhvatilov, and D.A. Tayurskii for useful discussions while preparing this paper. The study was supported by the Science and Technology Center in Ukraine, Project #5211.

References

1. E. Kim, M. Chan, Nature **427**, 225 (2004)
2. J. Day, J. Beamish, Nature **450**, 853 (2007)
3. X. Lin, A. Clark, M. Chan, Nature **449**, 1025 (2007)
4. M. Ray, R. Hallock, Phys. Rev. Lett. **105**(14), 145301 (2010)
5. B. Clark, D. Ceperley, Phys. Rev. Lett. **96**(10), 105302 (2006)

6. L. Pollet, M. Boninsegni, A. Kuklov, N. Prokof'ev, B. Svistunov, M. Troyer, Phys. Rev. Lett. **98**(13), 135301 (2007)
7. Y. Aoki, M. Keiderling, H. Kojima, Phys. Rev. Lett. **100**(21), 215303 (2008)
8. B. Hunt, E. Pratt, V. Gadagkar, M. Yamashita, A. Balatsky, J. Davis, Science **324**(5927), 632 (2009)
9. V. Grigor'ev, V. Maidanov, V. Rubanskii, S. Rubets, E. Rudavskii, A. Rybalko, Y. Syrnikov, V. Tikhii, Phys. Rev. B **76**(22), 224524 (2007)
10. I. Degtyarev, A. Lisunov, V. Maidanov, V. Rubanskiy, S. Rubets, E. Rudavskii, A. Rybalko, V. Tikhii, J. Exp. Theor. Phys. **111**(4), 618 (2010)
11. A. Andreev, JETP Lett. **85**(11), 714 (2007)
12. A. Balatsky, M. Graf, Z. Nussinov, S. Trugman, Phys. Rev. B **75**(9), 094201 (2007)
13. S. Sasaki, F. Caupin, S. Balibar, J. Low Temp. Phys. **153**, 43 (2008)
14. N. Mikhin, A. Polev, E. Rudavskii, JETP Lett. **73**(9), 470 (2001)
15. N. Mikhin, A. Polev, E. Rudavskii, Y. Vekhov, J. Low Temp. Phys. **148**(5/6), 707 (2007)
16. Y. Vekhov, A. Birchenko, N. Mikhin, E. Rudavskii, J. Low Temp. Phys. **158**, 496 (2010)
17. N. Mikhin, A. Birchenko, A. Neoneta, E. Rudavskii, Y. Vekhov, J. Phys.: Conf. Ser.–LT26 (to be published). arXiv:1106.6135
18. R. Toda, P. Gumann, K. Kosaka, M. Kanemoto, W. Onoe, Y. Sasaki, Phys. Rev. B **81**, 214515 (2010)
19. S. Kim, C. Huan, L. Yin, J. Xia, D. Candela, N. Sullivan, J. Low Temp. Phys. **158**, 584 (2010)
20. C. Huan, S. Kim, L. Yin, J. Xia, D. Candela, N. Sullivan, J. Low Temp. Phys. **162**, 167 (2011)
21. S. Kim, C. Huan, L. Yin, J. Xia, D. Candela, N. Sullivan, Phys. Rev. Lett. **106**, 185303 (2011)
22. A. Birchenko, E. Vekhov, N. Mikhin, K. Chishko, Low Temp. Phys. **35**(12), 914 (2009)
23. C. Pantalei, X. Rojas, D. Edwards, H. Maris, S. Balibar, J. Low Temp. Phys. **159**, 452 (2010)
24. H. Carr, E. Purcell, Phys. Rev. **94**(3), 630 (1954)
25. D. Miyoshi, R. Cotts, A. Greenberg, R. Richardson, Phys. Rev. A **2**(3), 870 (1970)
26. R. Guyer, R. Richardson, L. Zane, Rev. Mod. Phys. **43**, 532 (1971)
27. V. Grigor'ev, B. Esel'son, V. Mikheev, Sov. J. Exp. Theor. Phys. **37**(2), 309 (1973)
28. V. Grigor'ev, B. Esel'son, V. Mikheev, Sov. J. Exp. Theor. Phys. **39**(1), 153 (1974)
29. A. Allen, M. Richards, J. Schratter, J. Low Temp. Phys. **47**(3/4), 289 (1982)
30. N. Mikhin, A. Polev, E. Rudavskii, Y. Syrnikov, V. Shvarts, Low Temp. Phys. **26**, 395 (2000)
31. N. Bloembergen, E. Purcell, R. Pound, Phys. Rev. **73**(7), 679 (1948)
32. B. Cowan, *Nuclear Magnetic Resonance and Relaxation* (Cambridge University Press, Cambridge, 1997)
33. J.P. Korb, C. R. Phys. **11**(2), 192 (2010)
34. R. Wayne, R. Cotts, Phys. Rev. **151**(1), 264 (1966)
35. E. Hahn, Phys. Rev. **80**(4), 580 (1950)
36. H. Menges, H. Lohneysen, J. Low Temp. Phys. **84**(3/4), 237 (1991)
37. J. Bossy, T. Hansen, H. Glyde, Phys. Rev. B **81**(18), 184507 (2010)
38. A. Greenberg, W. Thomlinson, R. Richardson, J. Low Temp. Phys. **8**(1/2), 3 (1972)
39. H. Torrey, Phys. Rev. **92**(4), 962 (1953)
40. J. Franck, J. Jung, J. Low Temp. Phys. **64**(3/4), 165 (1986)
41. N. Mikhin, Low Temp. Phys. **30**, 429 (2004)
42. N. Mikhin, J. Low Temp. Phys. **138**(3/4), 817 (2005)
43. V. Naletov, M. Tagirov, D. Tayurskii, M. Teplov, J. Exp. Theor. Phys. **81**(2), 311 (1995)
44. E. Polturak, I. Schuster, I. Berent, Y. Carmi, S. Lipson, B. Chabaud, J. Low Temp. Phys. **101**(1/2), 177 (1995)